

Optical transport of sub-micron lipid vesicles along an optical nanofibre

Takaaki Yoshino^{1†}, Daichi Yamaura^{1†}, Maki Komiya^{1†}, Masakazu Sugawara¹, Yasuyoshi Mitsumori¹, Michio Niwano², Ayumi Hirano-Iwata¹, Keiichi Edamatsu¹, and Mark Sadgrove^{3*}

¹Research Institute of Electrical Communication, Tohoku University, Sendai 980-8577, Japan

²Kansei Fukushi Research Institute, Tohoku Fukushi University, 6-149-1 Kunimi-ga-oka, Aoba-ku, Sendai, Miyagi 989-3201, Japan

³Department of Physics, Faculty of Science, Tokyo University of Science, 1-3 Kagurazaka, Shinjuku-ku, Tokyo 162-8601, Japan

*mark.sadgrove@rs.tus.ac.jp

†These authors contributed equally to this work

ABSTRACT

Enhanced manipulation and analysis of bio-particles using light confined in nano-scale dielectric structures has proceeded apace in the last several years. Small mode volumes, along with the lack of a need for bulky optical elements give advantages in sensitivity and scalability relative to conventional optical manipulation. However, low particle index contrast, along with the complications caused by adhesion between particles and dielectric surfaces have meant that until now, nano-optics based trapping and transport of lipid-vesicles (e.g. liposomes) has not been achieved. Here we demonstrate the optical trapping and propulsion of sub-micron diameter liposomes along an optical nanofiber. Our results pave the way for integrated optical transport and analysis of composite bio-particles.

The ability to confine light to sub-wavelength volumes using index contrast or plasmonic excitations has led to the rapid adoption of micro- and nano-photonics in the detection, analysis and manipulation of small particles.¹⁻³ Of great practical interest is the use of such nanophotonic platforms for biological nanoparticles,⁴⁻⁹ where the ability to produce low-power, small-footprint, integrated optical devices can be expected to have a large impact in real-world applications. In particular, small mode volume optical resonators have already demonstrated impressive sensitivity in the detection of proteins^{4,7,10-12} and even viruses.^{4,13}

Nonetheless, many biological particles of interest consist of a membrane surrounding a liquid core making them difficult to manipulate optically in solution due to low index contrast. In addition, the membranes which define the boundary of such particles readily adhere to dielectric structures, making selective control impossible. Such particles include lipid vesicles and cells in general. Lipid vesicles known as liposomes are an excellent model for this class of particles and have a number of important applications including studies of cell movement,¹⁴ drug delivery,^{15,16} and synthetic cell creation¹⁷ to give just a few examples. Recent techniques have reduced the required power for optical manipulation of liposomes while extending techniques to smaller liposome sizes.¹⁸ However, although some recent research has used plasmonic methods to manipulate sub-micron liposomes,¹⁹⁻²¹ no direct nano-optical manipulation of individual sub-micron liposomes has been reported to date.

Here, we report the optically induced trapping and transport of sub-micron liposomes along an ultra-thin optical fibre (optical nanofibre). Small numbers of liposomes are confined near the surface of the fibre and propelled in the same direction as the optical mode propagation in the fibre. To the best of our knowledge, this is the first report of lipid vesicle transportation using a nano-optical device, and it is realized with low optical power (relative to free space methods) owing to the tight confinement of light in the optical nanofibre. Notable aspects of our results include the lack of adhesion of liposomes to the nanofibre and the fact that nanofibre diameters as low as 360 nm where necessary for optimal liposome transport, even though diameters close to 600 nm produce optimal field intensity at the nanofibre surface.

The situation we consider is as depicted in Fig. 1(a). A tapered fibre with a ~ 1 mm long waist region of diameter between 360 - 630 nm is immersed in a liquid solution containing liposomes. Light in the fibre's fundamental HE_{11} mode creates an evanescent field which penetrates deeply into the surrounding solution. A particle near the fibre experiences both a gradient force F_g which attracts the particle towards the fibre surface, and a light pressure force F_p which pushes the particle in the same direction as the nanofibre mode. As shown in Fig. 1(b), we model the liposomes as spherical lipid bilayers (index $n = 1.5$ ²⁷) containing pure water ($n = 1.33$), with a bilayer thickness of 5 nm. The lipid membrane includes rhodamine dye, allowing the

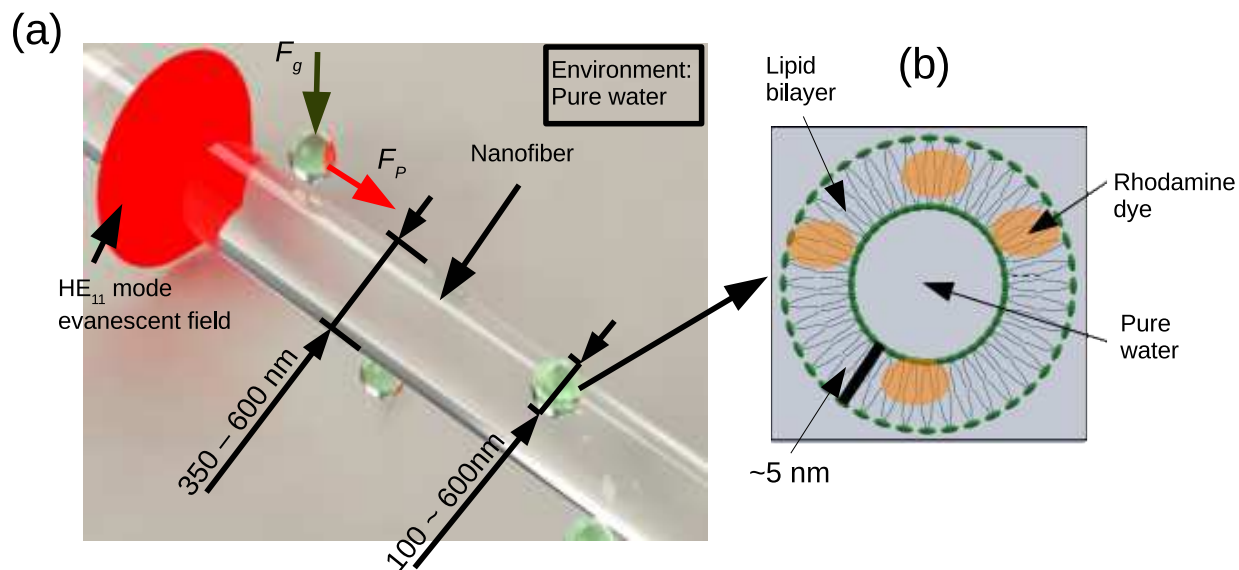


Figure 1. (a) Concept of the experiment. Liposomes (shown as green spheres) are trapped near the surface of the nanofiber by the evanescent field gradient force F_g and propelled in the same direction as the fiber mode due to its light pressure force F_p . (b) Schematic diagram of a unilamellar liposome tagged with rhodamine dye.

liposomes to be detected by fluorescence imaging.

Results

We characterized the size of the liposomes used in our experiments (prepared and measured as discussed in the Methods section), and found that the distribution was as shown in Fig. 2(a). The liposome diameter may be seen to be distributed between 100 nm and 600 nm with a broad peak between 150 nm and 300 nm. The liposome density in solution was found to be $\sim 12 \times 10^9 \text{ mL}^{-1}$.

The optical setup of our experiment is shown in Fig. 2(b). A nanofibre is prepared using a heat-and-pull method²⁹ and immersed in a droplet of solution containing liposomes. The transmission loss due to immersion is typically less than 10%. (Nanofibre diameter measurements are given in the Supplementary Material). To trap and transport liposomes near to the nanofibre surface, we introduce a 785 nm laser into the fibre. A separate laser at a wavelength of 540 nm is used to excite the rhodamine dye attached to the liposomes. The fluorescence from rhodamine has a broad spectrum with a peak near 580 nm and tails extending beyond 650 nm on the red side. We use two filters - a 600 nm cuton longpass filter and a 700 nm cutoff shortpass filter to cut the excitation and transport light leaving only the rhodamine photoluminescence from the liposomes. We checked that in the absence of the excitation laser, nothing is observed, while in the absence of the transportation laser, liposome brownian motion near the fibre can be seen, but no transport along the fibre is observed. This confirms that the optical trapping and transport effect is due to the 785 nm fibre mode.

Fig. 2(c) shows a series of images of a nanofibre (diameter 360 nm) immersed in a solution containing liposomes taken using the optical system shown in Fig. 2(a). The images show a liposome moving from left to right - the same direction as light propagation in the nanofibre. This data shows the trapping and transport of sub-micron liposomes by the evanescent field's gradient and scattering forces respectively. Here, we introduced white light illumination in addition to the two lasers shown in Fig. 2(a) to create the images, allowing the image of the nanofibre to be faintly seen. Note that we did not use white light illumination for the main experimental results reported here. Transport is seen to occur with almost no sticking of the liposomes to the fibre surface, despite the fact that, due to good lipid bilayer adhesion, silica is often used as a substrate to anchor lipid bilayer membranes.²⁴

Because of the effective one dimensional nature of transport along the nanofibre, we can combine all trajectories observed in the raw movie data into a single graph by layering the measured intensities along the fibre axis for each frame captured. Figure 3(a) shows such a summarized data set for the case where the nanofibre diameter was 360 nm and the optical power was 24 mW. This summarized raw data can be analyzed by approximating particle trajectories as straight line segments, allowing a velocity v and lifetime T_{trap} to be associated with each trajectory. Such processed data is shown in Fig. 3(b), where red dashed lines show the approximate straight line trajectory. 23 trajectories were identified in the case shown. From this analysis,

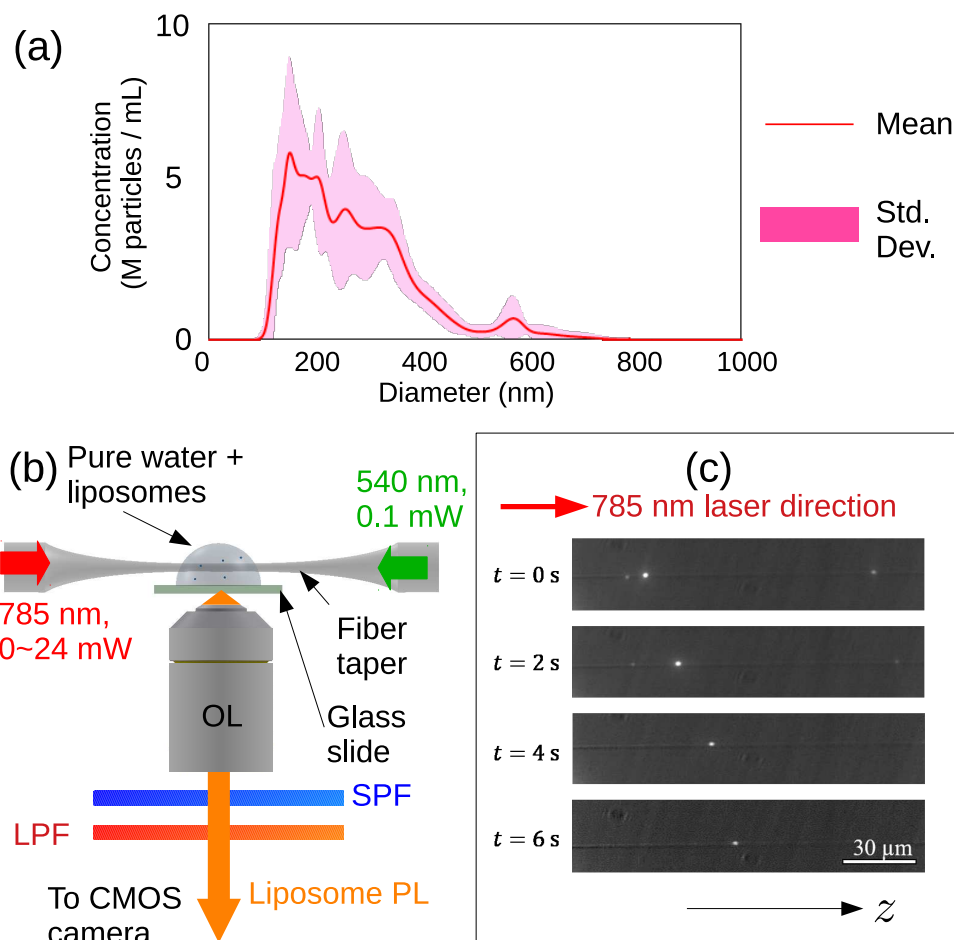


Figure 2. Experimental setup. (a) Data characterizing the diameter of liposomes in the sample. (b) Optical setup. A 785 nm laser injected into one end of the nanofibre provides the trapping and driving force, while a 540 nm laser injected into the opposite end excites the rhodamine dye in the liposome membranes. Light captured by an objective lens (OL) travels through a short pass filter (SPF, cut-off wavelength 700 nm) and a long pass filter (LPF, cut-on wavelength 600 nm) leaving only the rhodamine photoluminescence (PL) which is imaged by a complementary metal oxide semiconductor (CMOS) camera. (c) Frames from a movie recorded on the CMOS camera showing the movement of a liposome along the nanofibre.

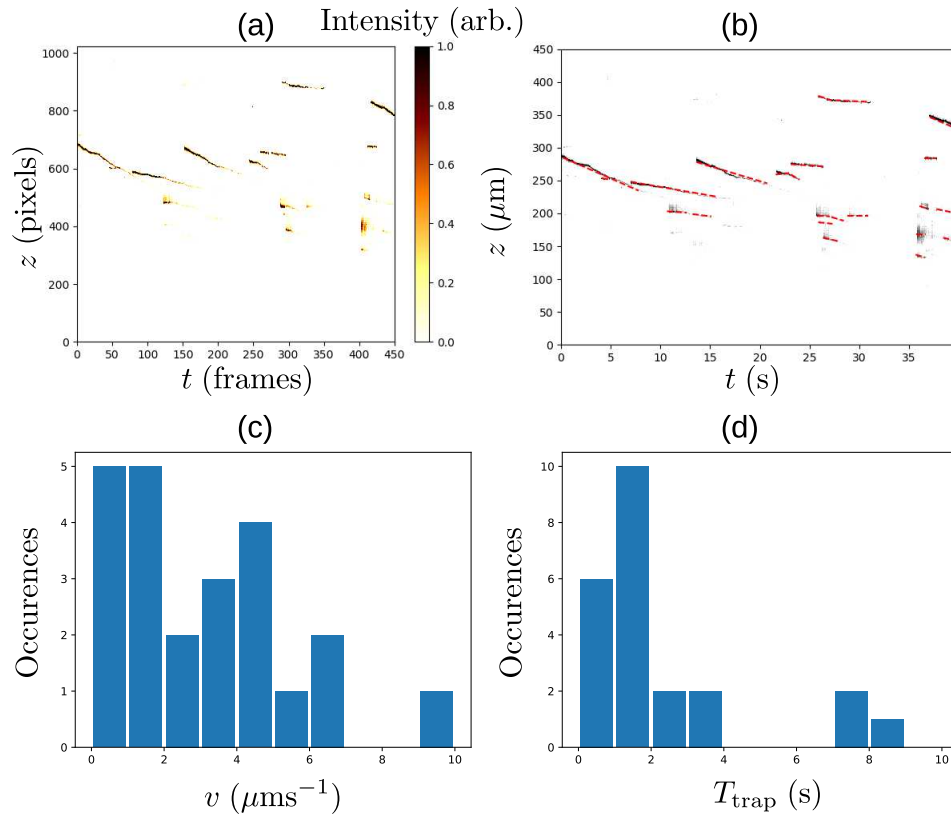


Figure 3. Observation of liposome transport along a nanofibre. (a) Raw data for a 360 nm diameter nanofibre. (b) Data with associated straight-line trajectories overlaid (red dashed lines). (c) Histogram of velocities associated with each trajectory in (b). (d) Histogram of trajectory lifetimes.

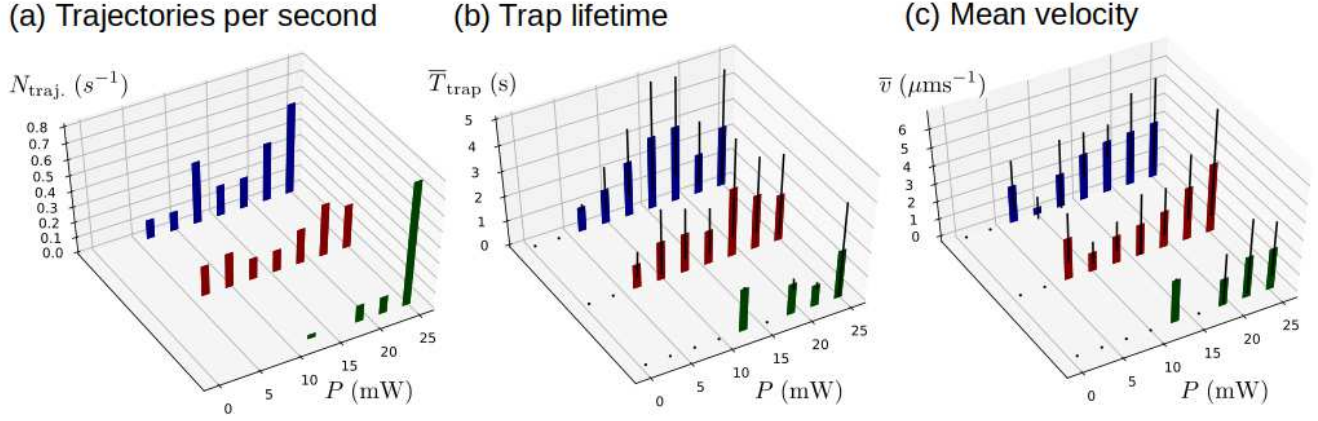


Figure 4. Power dependence of transport parameters for different nanofibre diameters. (a) Number of trajectories per second $N_{\text{traj.}}$ for nanofibre diameters of 360 nm (blue bars), 400 nm (red bars) and 550 nm (green bars). (b) Mean lifetimes \bar{T}_{trap} (bars) with black lines showing ± 1 standard deviation of the lifetime distribution. Nanofibre diameters are as in (a). (c) Mean velocities \bar{v} (bars) with black lines showing ± 1 standard deviation of the velocity distribution. Nanofibre diameters are as in (a).

the distribution of velocities and lifetimes may be extracted as shown in Figs. Fig. 3(c) and (d) respectively. Note that the liposomes in the sample had a wide range of diameters (150 nm - 600 nm) leading to a range of polarizabilities and thus optical forces. This leads to the wide distribution of velocities and lifetimes that we observed. Specifically, for the case shown in Fig. 3, the mean velocity \bar{v} was $3.1 \mu\text{ms}^{-1}$ while the standard deviation was $2.4 \mu\text{ms}^{-1}$. The mean trap lifetime (i.e. duration of the trajectory) was $\bar{T}_{\text{trap}} = 2.4$ s, while the standard deviation was 2.2 s.

We performed similar measurements for nanofibre samples of diameter 400 nm and 550 nm. (Additional measurements at a nanofibre diameter of 630 nm produced no trajectories within the observation time frame). Measurements were made at optical powers from 0 to 24 mW at intervals of 3 mW. Figure 4 presents a summary of the results from these experiments. In each figure, blue, red and green bars correspond to data from the 360 nm, 400 nm, and 550 nm diameter nanofibres respectively.

Figure 4(a) shows the number of trajectories per second $N_{\text{traj.}}$ detected during the experiment as a function of optical power for the three different nanofibre diameters. For example, $N_{\text{traj.}}$ for the case shown in Fig. 3 was $23/40 \text{ s} = 0.58 \text{ s}^{-1}$. Note that in cases where ostensible single trajectories showed sections with differing velocity, we approximated the trajectory as two or more linear segments. The number of trajectories is seen to fall as the power decreased, with a gradual fall off seen in the cases of 360 nm and 400 nm diameter nanofibres and a relatively abrupt falloff seen in the case of 550 nm diameter. It is notable that for the 360 nm and 400 nm diameter nanofibres, trapping and transport is observed for optical powers as low as 6 mW.

Figure 4(b) shows the mean lifetime as a function of optical power at each nanofibre diameter. Black lines show \pm one standard deviation of the measured lifetimes in all cases. The lifetimes also followed the expected falloff as the optical power was decreased. However, there is a large spread in the trapping lifetimes. As discussed before, this is mainly attributable to the spread of liposome diameters in the sample.

Trajectory mean velocities as a function of power are shown in Fig. 4(c) for each nanofibre diameter. Black lines show \pm one standard deviation of the measured velocities in all cases. The data for 360 nm and 400 nm diameters are similar within the experimental error, with values between 3 and $4 \mu\text{ms}^{-1}$ at 24 mW optical power, and falling below $2 \mu\text{ms}^{-1}$ at 6 mW optical power. As for the lifetimes, a large spread in velocities is seen which we attribute to the variation of liposome diameter. The 550 nm diameter fibre data shows smaller velocities over all, with a mean velocity of $2.4 \mu\text{ms}^{-1}$ at 24 mW, and falling to $1.6 \mu\text{ms}^{-1}$ at 18 mW. Below 18 mW, only a single trajectory was seen in the case of 12 mW optical power.

We note that both the number of trajectories and the trapping lifetimes are dependent on the optical gradient force F_g , whereas the velocity depends on the optical pressure force F_p .

Discussion

The results presented above clearly demonstrate the optically induced trapping and transport of liposomes along the surface of an optical nanofibre. This transport was achieved for moderate laser powers compared to liposome trapping using conventional optical tweezer techniques,¹⁸ with trapping and transport observed down to 6 mW optical power for the two thinnest nanofibre

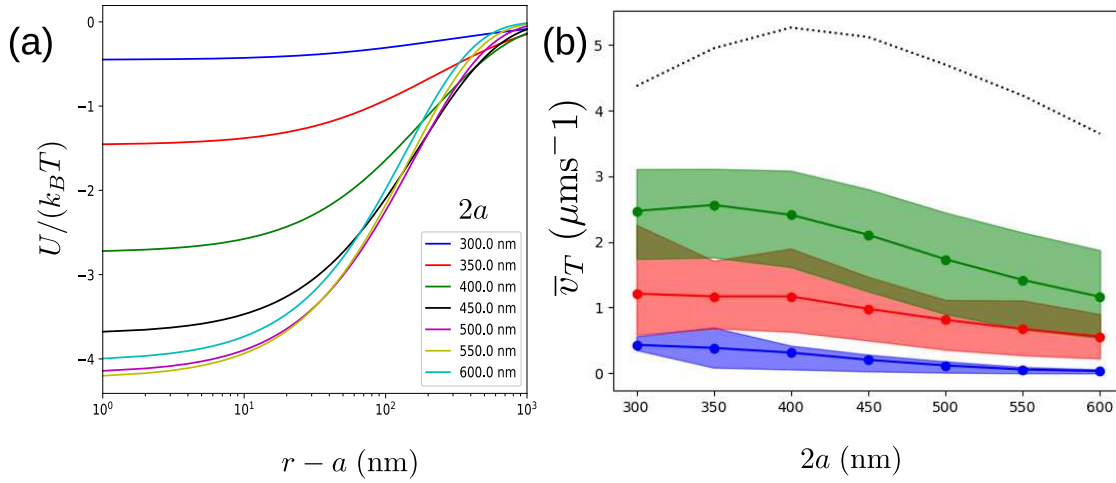


Figure 5. (a) Potential energy induced by the light gradient force on a 100 nm unilamellar liposome for the nanofibre diameters $2a$ as indicated in the legend. The potential is plotted against $r - a$ so that the zero point on the horizontal axis corresponds to the nanofibre surface. The electric field intensity outside the nanofibre surface is calculated at an azimuthal angle of 90° for a y -polarized HE_{11} mode of wavelength 780 nm. The mode power was set to 24 mW. (b) FDTD simulated average terminal velocities \bar{v}_T for unilamellar (blue line), bilamellar (red line) and trilamellar (green line) liposomes. \bar{v}_T was calculated for ten different liposome diameters between 100 nm and 600 nm. The shaded region in each case indicates the range of \bar{v}_T values from minimum to maximum. The black dotted line shows results for bilamellar liposomes when the lipid bilayer refractive index is set to 1.7.

samples. Our results extend numerous recent studies where thin optical fibres have been used to trap and propel micro and nanoparticles^{22,23} to the regime of composite, low index bio-nanoparticles.

Furthermore, we saw no significant adhesion of liposomes to the nanofibre surface on the time scale of the experiments (typically 30 minutes to 1 hour in total.) The reason why adhesion doesn't occur in the case considered here is still a subject of research. One important factor appears to be the background pure water environment. Evaluation of the exact environmental factors necessary to prevent adhesion will be the subject of future research.

The question of whether photo-thermal forces play a role in the observed trapping and transport of liposomes is important. In the highest power case considered here (24 mW of power in the fibre mode), let us assume that the 10% fall in transmission after the fibre was immersed in the liposome solution is entirely due to absorbed laser power. Then, solving the Poisson equation for temperature in a cylindrical geometry (see Supplementary Material), and assuming that the surface of the liquid surrounding the nanofibre is at room temperature gives a rise in temperature of 10 K relative to room temperature at the nanofibre surface. Estimating the temperature gradient along the fiber, as an upper limit, we can assume the temperature difference between the two ends of the nanofiber is 10 K, giving a temperature gradient of $\sim 10^4 \text{ K m}^{-1}$. This is three orders of magnitude smaller than the values reported recently by Hill *et al.*¹⁹ in which thermal trapping of liposomes was achieved. This suggests that thermal gradient based forces are not relevant to the transport part of our current experiment. On the other hand, a temperature rise of 10 K would reduce the water viscosity in the vicinity of the fibre surface by $\sim 12\%$ compared to room temperature. This leads to a similar percentage increase in the liposome velocity relative to room temperature. As for the radial temperature gradient, it can be estimated to be of order $1 \times 10^6 \text{ K m}^{-1}$ (see supplementary material), still an order of magnitude smaller than the largest gradients used by Hill *et al.*¹⁹ to thermally trap liposomes. Although this result does not rule out the possibility that thermal effects could play some role in trapping particles at the nanofiber surface, as we will show below, optical forces alone are sufficient to account for the observed behavior.

We now compare our experimental results with calculations of the optical force on liposomes near the nanofibre. Figure 5(a) shows the optical potential induced by the gradient force F_g of the nanofibre mode for a number of nanofibre diameters. Calculations were performed for a liposome of 100 nm diameter (at the edge of the Rayleigh regime) assuming a spherical liposome with a uniform index of 1.37, as calculated using a volume average of the outer membrane and the enclosed water and for 24 mW of optical power. For nanofibre diameters above 300 nm, the potential depth is seen to be comparable to or greater to $k_B T$ even for this small liposome diameter, and the depth of the potential ideally increases with the liposome radius cubed, implying that radial trapping of the liposomes in our sample can be readily achieved in agreement with our

experimental results.

The optical radiation pressure force F_p on the trapped liposomes is most accurately calculated by numerical simulations of Maxwell's equations. We used the finite-difference time-domain method (FDTD) to perform the force calculations. (Details are given in the supplementary material). Although the liposomes used in our experiment are predominantly unilamellar, it is expected that both bilamellar and trilamellar liposomes are present in the solution. Recently, using the same preparation method as that used here, Nele *et al.* reported percentages by number of 79, 14 and 6% for unilamellar, bilamellar and trilamellar liposomes respectively,²⁵ and a similar percentage composition is expected in our case. We therefore performed simulations for uni-, bi-, and trilamellar liposomes.

Assuming constant liposome velocity (i.e. terminal velocity in water), and neglecting the effect of the nanofibre, the pressure force can be converted into a velocity using Stokes law $F_p = 3\pi\Phi_l\eta v_T$, where Φ_l is the liposome diameter, $\eta = 8.9 \times 10^{-4}$ Pa·s is the dynamic viscosity of water at room temperature, and v_T is the liposome (terminal) velocity. Following our estimation of the temperature near the nanofibre surface, we adjust the velocities up by 12% to allow for the expected drop in viscosity. Figure 5(b) shows numerical calculations of the velocity in the case of unilamellar (blue line), bilamellar (red line) and trilamellar (green line) liposomes for nanofibre diameter $2a$ between 100 and 600 nm. The displayed values \bar{v}_T are averages over simulation results for liposome diameters between 100 and 600 nm, and the shaded region in each case indicates the range of v_T values from minimum to maximum. It is notable that the velocity increases as the nanofibre diameter decreases, with maximum velocities of approximately 0.4, 1.2 and $2.4 \mu\text{ms}^{-1}$ for uni-, bi- and trilamellar liposomes respectively. In addition, the effect of rhodamine dye on the lipid index at 780 nm is unknown, but is expected to increase the index to a value between 1.5 and 2.0.²⁶ For comparison, we show the case for bilamellar liposomes with a membrane index of 1.7 as a dotted black line in Figure 5(b). We note the trend in mean velocity as nanofibre diameter varies is in agreement with that observed in experiments. In particular the velocities seen in the case of 360 nm and 400 nm nanofibre diameters are higher on average than those seen in the case of 550 nm diameter. This is somewhat surprising, given that the nanofibre diameter which optimizes the surface intensity is ~ 600 nm for 785 nm input light. These results suggest that mode penetration into the surrounding solution is more important in determining the total light pressure force on liposomes than the maximum intensity at the nanofibre surface. Comparison with simulation results suggests that bilamellar and trilamellar liposomes are also trapped and transported in significant numbers in the experiment, leading to a higher mean velocity than would be expected from unilamellar liposomes alone. Indeed, due to their higher polarizability, bi- and trilamellar liposomes are more likely to be trapped and thus observed in the experiment.

In terms of quantitative agreement, we note that the maximum mean velocity predicted by simulations for trilamellar liposomes ($2.4 \mu\text{ms}^{-1}$) is close to the largest mean velocities seen in experiments ($3 \sim 4 \mu\text{ms}^{-1}$). The larger velocities in the case of experiments may be due to the increase of the membrane refractive index due to the presence of rhodamine.

In conclusion, we have demonstrated that sub-micron liposomes can be optically trapped and transported along the surface of an optical nanofibre. The lowest optical power at which trapping and transport was observed was at 6 mW for a 360 nm diameter nanofibre. As far as we are aware, this is the lowest optical power at which liposomes have been all-optically trapped and manipulated. Additionally, no significant adhesion of liposomes to the nanofibre was observed. The advantages of our technique over standard optical tweezers include the aforementioned low optical power, an uncomplicated optical setup, and the possibility of introducing multiple fields into the fibre, which can all be concentrated at the fibre waist regardless of wavelength. This last fact may be very useful when it comes to analysis of the contents of liposomes, exosomes and cells, leading to integrated nano optical manipulation and analysis tools for bioparticles. Furthermore, optical nanofibres are a mature platform for nanophotonics, including photonic crystal cavities.^{30,31} One intriguing possibility for future research using our technique is to couple liposomes and, eventually, living cells strongly to a nanophotonic cavity.⁸

Methods

Fiber preparation and insertion into liposome solution Tapered fibres were fabricated using a heat and pull process^{28,29} applied to commercial single mode optical fibre (780HP). The nanofibre was submerged in a $\sim 100 \mu\text{L}$ droplet of liposome solution (liposome density $\sim 12 \times 10^9 \text{ mL}^{-1}$) by touching the droplet to the fibre from below and then “sinking” the nanofibre in the droplet by pipetting a small amount ($\sim 10 \mu\text{L}$) of pure water from above.

Optical measurement We used a 50x objective (Nikon, Lu Plan Fluor 50x / NA 0.8) for observation of the nanofibre waist. The light from the lens was detected by a CMOS camera (Thorlabs DCC1545M). The liposome membrane was tagged with rhodamine dye whose optical absorption band exists near 550 nm, with an emission band near 600 nm. To excite the rhodamine and detect liposomes, we introduced a CW laser (wavelength 530 nm) into the nanofibre. To filter out the excitation light and any scattered light from the transport beam, we inserted two filters (600 nm long pass and 700 nm short pass) before the CMOS camera. For each optical power, we saved between 35 and 40 s of data as an avi format movie file.

Data processing To process the data, we first extract each frame from the raw movie data to separate image files. Secondly, we create 1D data from each image file by extracting pixels values along the line coinciding with the fibre position in the

image. We then agglomerate the 1D data into a single 2D data set which allows us to see the trajectories taken by individual liposomes. We then identify the start and endpoint of each trajectory and calculate the associated velocity and lifetime. In rare cases where an apparent single trajectory has sections with varying velocity, we approximate the trajectory by straight line segments, so that Stokes law can be applied to each segment.

Liposome sample preparation 3.925 mg of 1,2-dioleoyl-sn-glycero-3-phosphocholine (DOPC) (Avanti Polar Lipids, Inc.) and 0.006 mg of 1,2-dioleoyl-sn-glycero-3-phosphoethanolamine-N-(lissamine rhodamine Bsulfonyl) (Rhod-DOPE) (Avanti Polar Lipids, Inc.) were dissolved in chloroform in a glass vial. Chloroform was evaporated with a flow of nitrogen gas for 5 min and then evacuated in a vacuum desiccator for at least 6 h. The dried lipid films were rehydrated in 5 mL of pure water to give a lipid concentration of approximately 1 mM and vortexed for 1 h to prepare phospholipid multilamellar liposome suspensions. The liposome suspension was then repeatedly frozen and thawed five times with liquid nitrogen, and extruded five times through a polycarbonate membrane filter with a pore size of 400 nm (Merck Millipore Ltd.)^{24,32}

Liposome sample characterization The size distribution of the prepared liposomes was measured using a nanoparticle characterization system equipped with a 405 nm wavelength laser (NanoSight LM10-HSBFT14, Quantum Design Japan). The radius r of liposomes, was derived using the Stokes-Einstein equation $D_t = k_B T / 6\pi\eta r$ where k_B is Boltzmann's constant, T is the temperature, η is the viscosity of the liquid, and D_t is the diffusion coefficient. The value of D_t can be obtained based on the analysis of the Brownian motion of nanoparticles by the NTA technique. Measurements were carried out at room temperature in a cell installed in the NTA equipment.

Finite difference time domain simulations Detailed information regarding the simulations may be found in the supplementary material.

Data availability Data is available upon reasonable request.

References

1. Novotny, L., and Hecht, B., Principles of nano-optics. Cambridge university press, 2012.
2. Kawata, S. and Sugiura, T., “ Movement of micrometer-sized particles in the evanescent field of a laser beam”, Opt. Lett. **17**, 772 (1992).
3. Juan, M., Righini, M., and Quidant, R., “Plasmon nano-optical tweezers”, Nature Photon. **5**, 349–356 (2011).
4. He, L., Ozdemir, S. K., Zhu, J., Kim, W., and Yang, L., “Detecting single viruses and nanoparticles using whispering gallery microlasers”, Nat. Nanotechnol. **6**, 428–432 (2011).
5. Beuwer, M. A., Prins, M. W. J., and Zijlstra, P. “Stochastic protein interactions monitored by hundreds of single-molecule plasmonic biosensors” Nano Lett. **15**, 3507–3511 (2015),.
6. Rattenbacher, D., Shkarin, A., Renger, J., Utikal, T., Götzinger, S., and Sandoghdar, V. , “Coherent coupling of single molecules to on-chip ring resonators”, arxiv:1902.05257 (2019).
7. Baaske, M. D., Foreman, M. R. and Vollmer, F., “Single-molecule nucleic acid interactions monitored on a label-free microcavity biosensor platform”, Nat. Nanotechnol. **9**, 933 (2014).
8. Coles, D., Flatten, L. C., Sydney, T., Hounslow, E., Saikin, S. K., Aspuru-Guzik, A., Vedral, V., Kuo-Hsiang Tang, J., Taylor, R. A., Smith, J. M., and Lidzey, D. G., “A Nanophotonic Structure Containing Living Photosynthetic Bacteria”, Small **13**, 1701777 (2017).
9. Ashkin, A., Dziedzic, J. M. and Yamane, T., “Optical trapping and manipulation of single cells using infrared laser beams”, Nature **330**, 769–771 (1987).
10. Baaske, M., and Vollmer, F., “Optical resonator biosensors: molecular diagnostic and nanoparticle detection on an integrated platform”, Chem. Phys. Chem. **13**, 427–436 (2012).
11. Vollmer, F. et al. Protein detection by optical shift of a resonant microcavity. Appl. Phys. Lett. **80**, 4057–4059 (2002).
12. Foreman, M. R., Jin, W.-L., and Vollmer, F., “Optimizing detection limits in whispering gallery mode biosensing.” Opt. Express **22**, 5491–5511 (2014).
13. Vollmer, F., Arnold, S. and Keng, D., “Single virus detection from the reactive shift of a whispering-gallery mode”, Proc. Natl Acad. Sci. USA **105**, 20701–20704 (2008).
14. Somasundar, A., Ghosh, S., Mohajerani, F. et al. Positive and negative chemotaxis of enzyme-coated liposome motors. Nat. Nanotechnol. **14**, 1129–1134 (2019).
15. Mikhaylov, G., Mikac, U., Magaeva, A. et al. Ferri-liposomes as an MRI-visible drug-delivery system for targeting tumours and their microenvironment. Nat. Nanotechnol. **6**, 594–602 (2011).

16. Deng, W., Chen, W., Clement, S. et al. Controlled gene and drug release from a liposomal delivery platform triggered by X-ray radiation. *Nat. Commun.* **9**, 2713 (2018).
17. Godino, E., López, J.N., Foschepoth, D. et al. De novo synthesized Min proteins drive oscillatory liposome deformation and regulate FtsA-FtsZ cytoskeletal patterns. *Nat. Commun.* **10**, 4969 (2019).
18. Bendix, P. M. and Oddershede, L. B., “Expanding the Optical Trapping Range of Lipid Vesicles to the Nanoscale”, *Nanoletters* **11**, 5431 (2011).
19. Hill, E. H., *et al.* “Opto-Thermophoretic Attraction, Trapping, and Dynamic Manipulation of Lipid Vesicles” *Langmuir* **34**, 13252-13262 (2018).
20. Kuboi M., Takeyasu, N., Kaneta T., “Enhanced Optical Collection of Micro- and Nanovesicles in the Presence of Gold Nanoparticle” *ACS Omega* **3**, 2527-2531 (2018).
21. Tani, Y., Kaneta, T., “Enhancement of optical force acting on vesicles via the binding of Gold nanoparticles”, *Royal Society Open Science* **6**, 190293 (2019).
22. Maimaiti, A., *et al.* Higher order microfiber modes for dielectric particle trapping and propulsion. *Sci Rep* **5**, 9077 (2015).
23. Skelton, S. E. *et al.*, “Evanescent wave optical trapping and transport of micro- and nanoparticles on tapered optical fibers”, *J. Quant. Spectrosc. Radiat. Transf.* **113**, 2512–2520 (2012).
24. Yamaura, D., *et al.*, “Amphiphobic Septa Enhance the Mechanical Stability of Free-Standing Bilayer Lipid Membranes”, *Langmuir* **34**, 5615-5622 (2018).
25. Nele, V., Holme, M. N., Kauscher, U., Thomas, M. R., Douthett, J. J., and Stevens, M. M., “Effect of formulation method, lipid composition and PEGylation on Vesicle lamellarity: A small angle neutron scattering study”, *Langmuir* **35**, 6064 (2019).
26. Alnayli, R., Shanon, S., and Hadi, A., “Study the Linear and Nonlinear Optical Properties for Laser Dye Rhodamine B”, *J. Phys.: Conf. Series* **1234** 012022, (2019).
27. Matsuzaki, *et al.*, *Biochimica et Biophysica Acta* **1467** 219-226 (2000).
28. Birks, Timothy A., and Youwei W. Li. ”The shape of fiber tapers.” *Journal of Lightwave Technology* **10** 432-438 (1992).
29. Ward, J. M., Maimaiti, A., Le, V. H., and Nic Chormaic, S., “Optical micro- and nanofiber pulling rig” *Rev. Sci. Instrum.* **85** 111501 (2014).
30. Yalla, R., Sadgrove, M., Nayak, K. P., and Hakuta, K., “Cavity quantum electrodynamics on a nanofiber using a composite photonic crystal cavity”, *Phys. Rev. Lett.* **113**, 143601 (2014).
31. Nayak, K. P., *et al.*, “Nanofiber quantum photonics”, *J. Opt.* **20** 073001 (2018).
32. MacDonald, R. C, MacDonald, R. I., Menco, B. P. M., Takeshita, K., Subbarao, N. K., Hu, L. R., “Small-Volume Extrusion Apparatus for Preparation of Large, Unilamellar Vesicles”, *Biochim. Biophys. Acta - Biomembr.* **1061**, 297–303 (1991).

Acknowledgements

T. Y. acknowledges support from The Tanaka Kikinzoku Memorial Foundation scholarship, and The Ushio Foundation scholarship. M. S. acknowledges support from JSPS KAKENHI (Grant no. JP17H05460) in Scientific Research on Innovative Areas “Nano-material optical-manipulation” and is grateful to T. Kaneta for stimulating discussions regarding the optical manipulation of liposomes. We thank T. Ma for helping us to measure the size distribution of the liposomes. This research was partially performed using the facilities of the Fundamental Technology Center, Research Institute of Electrical Communication, Tohoku University.

Author contributions

TY manufactured nanofibers, set up part of the experiment, performed the optical experiments, and analysed the data. DY and MK prepared liposome samples. M. Sugawara contributed to nanofiber based parts of the experiment. YM contributed to the optical part of the experiment and co-supervised the research. MN performed measurements on the size and concentration of the liposomes. M. Sadgrove, AH and KE conceived of the original experiment and co-supervised the experiment. M. Sadgrove set up part of the experiment, performed preliminary measurements, performed simulations, and contributed to the analysis of the results. All authors discussed and contributed to writing the manuscript.

Additional information

Correspondence regarding the paper should be addressed to Mark Sadgrove.

Supplementary material

Finite difference time domain simulations

Here, we provide more details regarding the numerical simulations of the light pressure force imposed by the fibre mode on the liposomes. This is the force which causes the liposomes to move along the nanofibre in the same direction as the mode propagation. The nature of the liposomes brings a number of challenges when performing simulations. In particular, we note the following: i) the low index contrast between the liposomes and the surrounding water means that the preferred (and memory efficient) method of calculation - the Maxwell stress tensor - is not suitable, ii) the lamellarity of individually trapped and transported liposomes is unknown and iii) the rhodamine introduced to the lipid layer causes an unknown increase in the liposome refractive index. We now consider these points in order:

First, it is well known that for very low refractive index contrasts, such as that between liposomes and water, the Maxwell stress tensor, which is typically used for the numerical evaluation of optical forces for particles outside the Rayleigh range, is prone to large errors. Instead, we performed numerical evaluation of the optical forces on liposomes near the nanofibre surface by evaluating the Lorentz force throughout a $1 \mu\text{m}^3$ volume which included the liposome but excluded the nanofibre. Second,

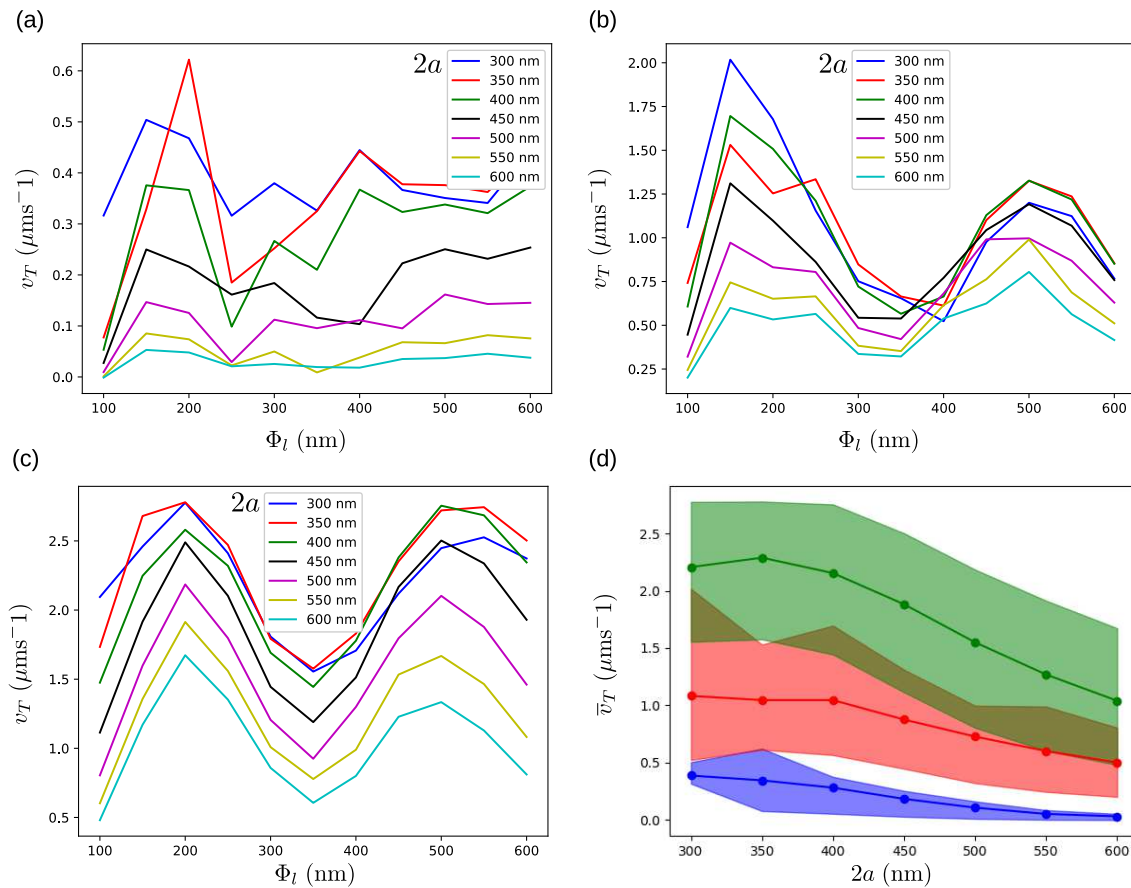


Figure 6. (a) Numerically calculated terminal velocities as a function of unilamellar liposome diameter for various nanofibre diameters as indicated in the legend. (b) Same as (a) but for bilamellar liposomes. (c) Same as (a) but for trilamellar liposomes. (d) Average velocities over liposome diameter as a function of nanofibre diameter $2a$, for unilamellar (blue circles), bilamellar (red circles) and trilamellar (green circles) liposomes. Lines are included to guide the eye. The shaded region in each case indicates the range of v_T values from minimum to maximum.

we model the liposomes as 5 nm shells of dielectric material of index $n_l = 1.5^{27}$ encasing pure water ($n_w = 1.33$). Although the liposomes are predominantly unilamellar, it is expected that both bilamellar and trilamellar liposomes are present in the

solution. Recently, using the same preparation method as that used here, Nele *et al.* reported percentages by number of 79, 14 and 6% for unilamellar, bilamellar and trilamellar liposomes respectively,²⁵ and a similar percentage composition is expected in our case.

Third, the liposomes are tagged with rhodamine-B dye to allow their detection by photoluminescence measurements. The addition of rhodamine dye is expected to cause an increase in refractive index of the lipid membrane. In particular, Alnayli *et al.* have reported values of refractive index above 710 nm for Rhodamine B in solution of between 1.5 and 2.0 depending on concentration.²⁶ Although an exact measurement of the refractive index of the lipid membrane of the liposomes used in our experiment is beyond the scope of the present paper, it is necessary to consider the possible range of refractive index when comparing experiment and simulations.

The numerical simulations of the light pressure force F_P on the liposomes were performed using the finite difference time domain method (Lumerical FDTD). We converted the force into a velocity by assuming that the light pressure force was balanced by the viscous force of the water, and using Stokes formula $F_P = 3\pi\Phi_l\eta v_T$, where Φ_l is the liposome diameter, $\eta = 8.9 \times 10^{-4}$ Pa·s is the dynamic viscosity of water at room temperature and v_T is the liposome (terminal) velocity. (Note that in the main paper, we adjusted the velocities to allow for the 10 K increase in temperature expected at the fibre surface, which leads to a $\sim 12\%$ decrease in viscosity relative to room temperature, and an associated $\sim 12\%$ increase in the calculated velocity).

The velocity is shown as a function of liposome diameter for unilamellar liposomes in Fig. 6(a) for various nanofibre diameters (NFDs) as indicated in the legend. We see that the mean velocity increases as the nanofibre diameter is decreased from 600 nm to 300 nm. The maximum velocity of $\approx 0.6 \mu\text{ms}^{-1}$ is seen to occur when the fibre diameter is 350 nm, and the liposome diameter is 200 nm. In Fig. 6(b), the same results are shown for the case where the liposome is bilamellar (i.e. the lipid membrane is twice as thick). Roughly the same trend is seen with increasing velocity as the nanofibre diameter is decreased from 600 nm to 300 nm. However, the average value of the velocity is approximately three times that seen for unilamellar liposomes. The maximum value of about $2 \mu\text{ms}^{-1}$ occurs for a nanofibre diameter of 300 nm and a liposome diameter of 150 nm. Additionally, two broad peaks in the velocity are seen near values of $\Phi_l = 200$ nm and $\Phi_l = 500$ nm. In Fig. 6(c) shows the same calculations in the case of trilamellar liposomes. Here we see average velocities about 5 times higher than the unilamellar cases with a maximum velocity of about $2.7 \mu\text{ms}^{-1}$ seen for $\Phi_l = 200$ nm and 500 nm, and for a nanofibre diameter of 350 nm. Finally, In Fig. 6(d) We show a summary of the data in (a)-(c) by plotting mean velocities over liposome diameter as a function of the nanofibre diameter $2a$.

Estimation of temperature at the nanofiber surface

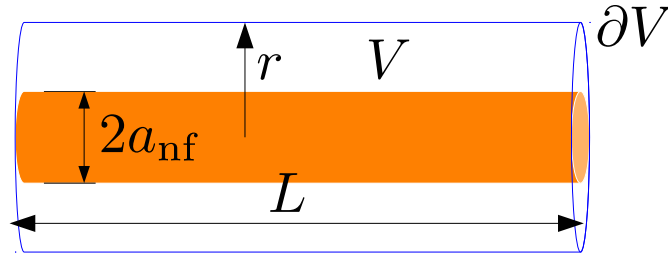


Figure 7. Schematic diagram of the system we consider in order to evaluate the temperature rise due to absorbance of laser light from the fibre mode. A region of diameter a_{nf} and length L is considered to have a constant power density ρ . We solve the Poisson equation for a cylindrical volume V with surface ∂V outside the constant power region with radius $r > a_{\text{nf}}$.

We estimated the temperature at the nanofibre surface and the temperature gradient experienced by liposomes using a simplified model of a cylindrically symmetric heat source (light absorbed from the guided mode of the nanofibre) as shown in Fig. 7. Assuming an infinitely long nanofibre (in our case, since the nanofibre length is much longer than its radius, this is not a bad approximation), the Poisson equation for the temperature T is

$$\nabla^2 T = \begin{cases} -\frac{\rho}{\lambda}, & r < a_{\text{nf}} \\ 0, & r > a_{\text{nf}} \end{cases}, \quad (1)$$

where $\rho = 2.4 \text{ mW}/(2\pi(500 \text{ nm})^2 \times 1 \text{ mm})$ is the power density defined as the total absorbed power within the region of radius a_{nf} and over the 1 mm region where the nanofibre is at its thinnest, and $\lambda = 0.592 \text{ W/m.K}$ is the thermal conductivity of water.

It is simplest to first use Gauss' law to solve for the gradient of the temperature:

$$\begin{aligned}
\oint_{\partial V} \nabla T \cdot d\mathbf{A} &= \int_V -\frac{\rho}{\lambda} dV \\
\Rightarrow 2\pi r L (\nabla T)_r &= -2\pi \frac{\rho a_{\text{nf}}^2 L}{\lambda} \\
\Rightarrow \frac{\partial}{\partial r} T &= -\frac{\rho a_{\text{nf}}^2}{\lambda r}.
\end{aligned} \tag{2}$$

Integrating Eq. 2 gives a general solution for T :

$$T(r) = -\frac{\rho a_{\text{nf}}^2}{\lambda} \log(r) + C. \tag{3}$$

The constant C can be determined by imposing an appropriate boundary condition. Here, we will assume that at the surface of the water droplet, a radial distance R from the fibre center, the water is at room temperature T_0 . This leads to the equation

$$C = T_0 + \frac{\rho a_{\text{nf}}^2}{\lambda} \log(R). \tag{4}$$

Finally, we find that the temperature difference ΔT between the fibre surface and room temperature can be written

$$\Delta T(r) = \frac{\rho a_{\text{nf}}^2}{\lambda} \log\left(\frac{R}{r}\right). \tag{5}$$

Taking a_{nf} to be 500 nm, and R to be 1 mm, we find that $\Delta T \approx 10$ K. This value is insensitive to the exact values of a_{nf} and R , being sensitive instead to the difference in their orders of magnitude due to the logarithmic dependence.

The temperature gradient in the radial direction can now be calculated. As a representative example, we set the nanofiber radius to $a_{\text{nf}} = 400$ nm, and choose a liposome diameter $\Phi_l = 300$ nm. Then, using Eq. 2, the temperature gradient at the center of the liposome is found to be about $3 \times 10^6 \text{ K m}^{-1}$.

The gradient along the nanofiber is more difficult to model accurately. As an upper bound, we can assume the the entire temperature gradient ΔT occurs along the ~ 1 mm length of the nanofiber. Then, in a one dimensional approximation, the temperature gradient is $10\text{K}/1\text{ mm} = 10^4 \text{ K m}^{-1}$.

Nanofibre diameter measurements

Here, we show typical results for diameter measurements of optical nanofibres. The measurements were made after the experiment was finished and the nanofibres had been removed from the liposome solution.

Fig. 8(a) shows a scanning electron microscope image taken of the nanofibre within the region of smallest diameter (the “waist” region). By taking such images along the length of the nanofibre, we can measure its diameter profile. Such a profile over a ~ 1 mm range is shown in Fig. 8(b). The nanofibre diameter is sub-micron over this range, and liposome transport along with heating of the water due to absorbance from the fibre mode can in principle happen anywhere along this region. Fig. 8(c) shows the sam data as Fig. 8(b), but zoomed in to the region near the nanofibre waist.

Liposome size measurements

Here we display extra diameter characterization data for liposomes extruded through a 100 nm polycarbonate membrane filter. We first show the data presented in the main paper (Fig. 2(a)) to allow easy comparison.

Fig. 9(a) shows the diameter characterization data for liposomes filtered through a 400 nm polycarbonate membrane as used in the experiments whose results are given in the main paper. We also attempted experiments with liposomes filtered through a 100 nm polycarbonate membrane (diameter characterization shown in Fig. 9(b)) but for that liposome sample, no transport behavior was observed, suggesting that transport occurs predominantly for liposomes with diameter greater than 100 nm.

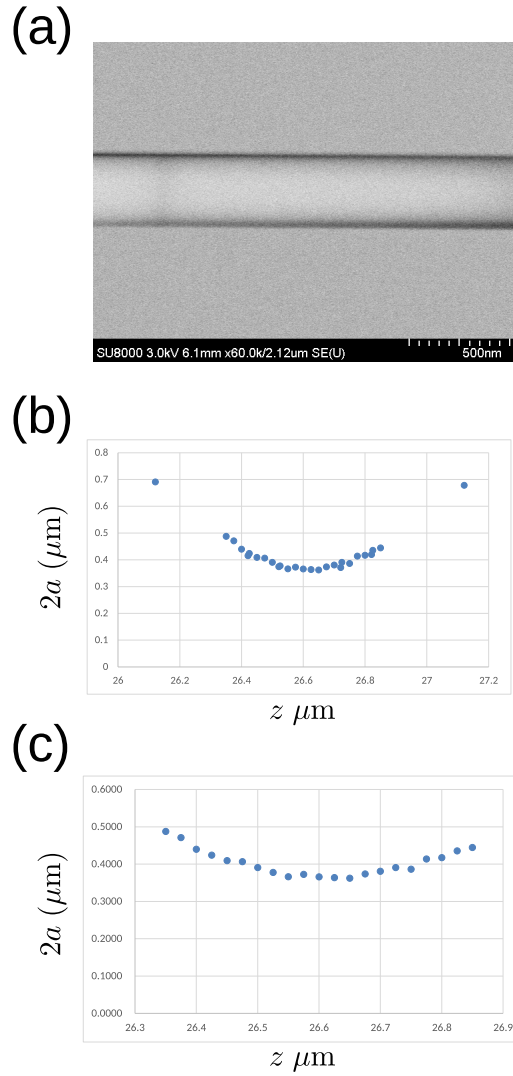


Figure 8. (a) Scanning electron microscope of nanofibre used in experiments in its waist region. (b) Diameter measurements of the nanofibre over a ~ 1 mm range. (c) Diameter measurements over the nanofibre waist region.

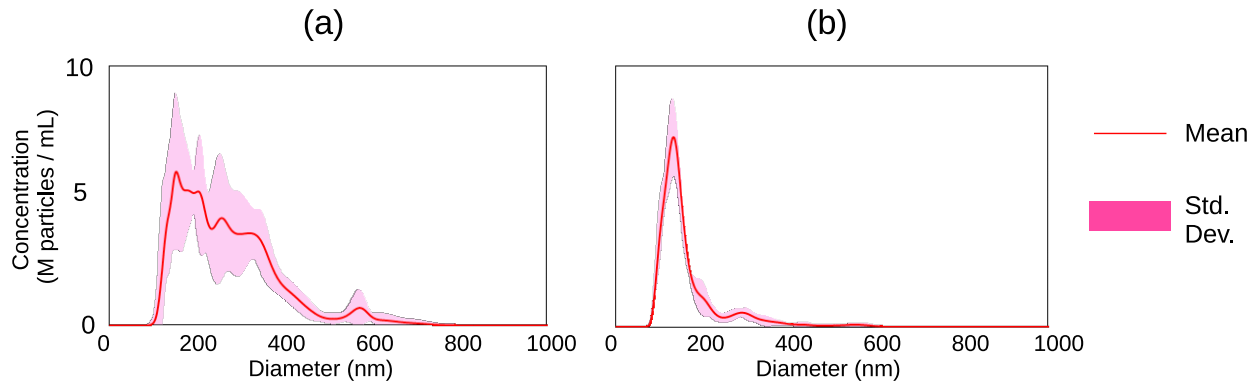


Figure 9. (a) Diameter characterization of liposomes used in our experiments. (b) Diameter characterization of liposomes filtered with a 100 nm polycarbonate membrane.